scientific reports

Check for updates

OPEN

The effect of adipose tissue on transdermal monochromatic light presented to the human fetus using Monte Carlo simulations

Zac Isaac[1]✉, Jacob Heerikhuisen[1] & Vincent Reid[2]

The extent to which transdermal light sources illuminate the uterine environment is unknown. Recent work indicates the human fetus responds to external visual stimuli, such as laser diodes, and initial modeling suggests the fetus may not develop in a completely dark environment as previously assumed. Development of the human visual system begins within the womb, and there is motivation in fields such as developmental psychology, transabdominal oximetry, and photoacoustics to explore the extent to which light penetrates maternal abdominal tissue and understand how transdermal stimuli appear to the fetus. We develop and adapt a Monte Carlo model utilising third trimester histological properties of maternal tissue to simulate transdermal monochromatic collimated light sources, with particular focus on the 650 nm wavelength used in experimental applications. We determine approximate levels of third trimester uterine illumination from such stimuli, ranging from being comparable to an overcast night to a full moon in clear conditions. We further discuss the scope for multiple stimuli to be visibly distinct in utero for experimental applications. This modeling provides quantitative guidance on the interactions between transdermal monochromatic collimated source laser diode stimuli and maternal tissue to practitioners and researchers in the fields of fetal vision, ultrasound, and developmental psychology.

Little is known about how the human fetus engages with the visual world. Several studies have shown evidence of fetal sensory stimulation in the uterus through auditory or olfactory stimuli[1,2], yet the presence of uterine visual stimulation from external light sources has been consistently assumed as either absent or negligible[3]. Historically, circumstances allowing for illumination of the uterus were suggested to be limited to cases where the maternal abdomen was exposed directly to a powerful light source[4]. Accordingly, research in the field of fetal visual development has been limited, though some experimental work has suggested there is sufficient light entering the uterine environment of pigs and guinea pigs to allow for fetal visual stimulation[5].

More recently, work exploring the human visual experience prior to birth utilized quantitative modeling to assess the visual environment for the human fetus during the final two months of gestation, with results indicating many fetuses may develop in conditions providing sufficient illumination of the uterine cavity for visual experience[6]. This finding renewed experimental research interest in fetal visual development, with later studies presenting diode light sources to the fetus through the maternal abdomen and concluding that fetuses show a preference for face-like stimuli[7].

Subsequent research found that uterine light is essential for the typical formation of the eye in mice[8]. This raised the question of whether light was required for all mammalian visual systems during gestation. As it is not ethically appropriate to conduct experiments with humans where the visual system may become impaired, further work explored the impact of naturalistic variation in average day length (hence, natural light exposure) during early human gestation and the associated visual outcomes for infants[9]. Findings suggested that there may be impacts to the human visual system from the number of daylight hours.

It is clear that the development of research within the field of fetal vision, combined with our growing knowledge of the uterine visual environment, has indicated the need for targeted research into the levels of light stimuli present within the human uterus across gestation. More generally, such research provides benefit to those working in transabdominal oximetry and photoacoustics through a greater understanding of the effects of tissue components on transdermal light and how stimuli might present to the fetus.

[1]Department of Mathematics, University of Waikato, Hamilton, New Zealand. [2]School of Psychology, University of Waikato, Hamilton, New Zealand. ✉email: zac.isaac@waikato.ac.nz

To our knowledge, modeling of light that reaches the human fetus has been limited to four previous forms of approach.

First, perturbation methods have been used to model photon transport through the fetus (a prominent example models transport through the brain[10]); however, researchers in these areas are typically not concerned with uterine illumination or stimuli appearance to the fetus — both of interest in developmental psychology.

Second, general illumination of the uterine cavity has been modeled by measuring light transmission through biological tissue samples and estimating a regression equation[6]. This approach demonstrated that the uterus may be an environment allowing for visual experience under certain conditions, though the method lacked flexibility and offered only an isolated snapshot of the conditions measured with the tissue samples. Any variation in optical tissue properties such as absorption or scattering coefficients would impact the physical processes occurring during light propagation and cause results to deviate from the model's predictions. More thorough modeling is hence needed to develop this work.

Third, in response to claims of fetal preference for face-like stimuli in the womb[7], outputs from Monte Carlo (MC) simulations were used to demonstrate the apparent difficulty for the fetus in distinguishing the presented stimuli[11]. This approach explicitly modeled the appearance of transdermal stimuli to the fetus; however, one drawback was the limited application and investigation of the work (though this was not the overall intention of the paper). The authors employed a single instance of a one-layer tissue model and the maternal abdominal tissue was assumed to be homogeneous. In reality, maternal tissue is composed of multiple constituent layers — each with different optical properties — and the assumption of a homogeneous medium may omit impacts due to the varying nature of the tissue across layers. The field would benefit from a deeper investigation of these impacts and the extent to which transdermal stimuli may be used in future fetal visual development studies.

Fourth, in transabdominal fetal monitoring (and similar fields), computational modeling has been employed to simulate light transport to the fetus for observation of fetal wellbeing. For example, various efforts have been made in fetal pulse oximetry to model light transport in maternal tissue; recently, MC simulations were used to determine the effect of amniotic fluid on recovering fetal signals through the maternal abdomen[12]. In this work, researchers utilize a three-layer maternal tissue model and vary the subdermal layer, though their focus (and that of others in these fields) is on aspects not directly related to our interests. Such works also typically explore signals at wavelengths outside the range of those used in experimental fetal vision research, where studies focus on wavelengths that can be perceived by the fetal eye as estimated by newborn capacities.

Further, fetal visual development research currently focuses on the third trimester of pregnancy due to the late development of the fetal eye, with previous research showing the fetal brain responds to light during the third trimester[13] and the fetus moves its eyes at 34 weeks in response to the introduction of transdermal light stimuli on the mother's abdomen[14]. Hence, in order to further inform and develop these experimental applications, model parameters need to be relevant to this stage of pregnancy. No previous research addresses this consideration when modeling how transdermal stimuli appear to the fetus or the levels of uterine illuminance provided.

Inspection of the basic component layers of maternal abdominal tissue (skin, adipose, muscle, and uterus) highlights the primary motivation of this research. From empirical studies[15–17], the layer that generally exhibits the greatest thickness and variation in thickness across individuals in their third trimester of pregnancy is adipose tissue. In addition, adipose is the layer which generally has the most profound impact on the propagation of light to the womb. This can be seen by inspection of the optical properties sourced from literature in Tables 1–3. It is clear that adipose tissue is highly photon-absorbing relative to most other tissue layers, thus more heavily diminishing the levels of light reaching the womb. Similarly, average layer thicknesses taken from empirical studies show adipose tissue thickness in pregnant women to typically vary from 1.0 cm to 2.0 cm. In combination with the highly photon-absorbing nature of this tissue, the implication is that adipose plays an important role in determining the levels of light reaching the fetus, and a large amount of uterine light variation across individuals is influenced by variations in adipose tissue.

In order to model the amount of light that reaches a human fetus from the application of monochromatic collimated source stimuli to the exterior maternal abdomen, we present a computational model developed in C17 standard C that implements a direct particle simulation MC approach to simulate light transport through dynamically dispersive tissue. The model incorporates five layers, with four representing the maternal tissues and one representing the amniotic fluid. All simulations have been run with at least 12 billion photon packets to reduce noise and generate appropriate statistical accuracy. We adjust the model's adipose layer by varying its

nm	Skin[24,25]	Adipose[25,26]	Muscle[27]	Uterus[28,29]	Am. Fluid[30]
400	3.76	3.90	8.00	1.64	0.0002
450	2.50	2.00	5.67	1.26	0.0004
500	1.19	1.30	4.00	0.95	0.0005
550	1.25	1.40	2.65	0.70	0.0008
600	0.69	0.90	1.70	0.50	0.003
650	0.14	0.70	1.20	0.35	0.003
700	0.48	0.60	0.48	0.20	0.006

Table 1. Absorption coefficients, μ_a [cm^{-1}], used in Monte Carlo simulations for each wavelength (listed as, and measured in, nm) and medium. Emphasis is placed on using values relevant to women in the third trimester of pregnancy (or those that most accurately represent this situation).

nm	Skin[24,25]	Adipose[25,26]	Muscle[31]	Uterus[28,29]	Am. Fluid
400	626.94	178.66	146.43	180.00	1.00†
450	460.46	165.00	129.48	171.40	1.00
500	363.80	153.51	115.98	163.00	1.00
550	304.11	144.00	104.98	152.60	1.00
600	265.29	135.61	95.86	141.00	1.00
650	90.08	128.43	88.17	137.00	1.00
700	220.21	122.00	81.60	113.00	1.00

Table 2. Scattering coefficients, μ_s [cm^{-1}], used in Monte Carlo simulations for each wavelength (listed as, and measured in, nm) and medium. Emphasis is placed on using values relevant to women in the third trimester of pregnancy (or those that most accurately represent this situation). † Assumed for all wavelengths. Researchers have used this value in MC simulations for longer wavelengths in the visible spectrum[12], though modeling of shorter wavelengths in amniotic fluid is limited.

	Skin	Adipose	Muscle	Uterus	Am. Fluid
g	0.90†	0.90	0.90	0.90	0.99[11]
n	1.40†	1.40	1.40	1.40	1.35[11]
t	0.20[24]¶	1.00-2.50[15–17]§	0.48[32]	0.60[33]¶	25.00*

Table 3. Optical anisotropies (*g*), refractive indices (*n*), and tissue thicknesses (*t* [cm]) used in Monte Carlo simulations for each medium across every wavelength. All values are sourced directly from literature where possible, though it is noted when an approximation has been made. Emphasis is placed on using values relevant to women in the third trimester of pregnancy (or those that most accurately represent this situation). † These values are used for all tissue layers. They are commonly found within ranges seen in literature.[11,24,25,27,34]. § This range also covers a large component of that seen in our experimental work. ¶ These values have been slightly altered to fit our voxel gridding. * Chosen to provide a large packet propagation area.

thickness, which addresses two aspects of pregnancy. First, across gestation, the structure of maternal abdominal tissue changes in response to the growing size of the fetus — i.e., there is a temporal aspect to consider when determining the illumination of the uterus. Adjusting the thickness of the adipose layer is a simple manner through which to initially explore this evolution. Second, this gives an insight into how body fat indicators may affect the illumination of the womb. For example, mothers with higher BMI values might be expected to have greater adipose tissue thickness, while the converse may be expected for mothers with lower BMI values. Consequently, these simulations highlight the extent to which uterine illumination levels from direct collimated source stimuli vary across the population with respect to such measures.

We further explore an application to a problem faced by developmental psychologists. As this field seeks to display distinct light sources to the fetus (such as moving two separate monochromatic collimated source light stimuli towards one another along the maternal abdomen exterior during presentation to the fetus), constraints require that the light sources, as viewed by the fetus, remain visibly distinct from one another — i.e., minimal stimuli merging visible to the fetal eye, and with a reduced concern for whether the original shape remains distinct (in contrast to earlier fetal visual work[7]). One of the things we are interested in exploring, then, is the point at which two such stimuli cease to become notably distinct from each other, with conclusions from this work being used to inform experimental design in future research.

Thus, in this paper, we aim to answer the following questions: (a) Is there a wavelength (or range of wavelengths) that increase likelihood of fetal visibility? (b) To what extent does such a transdermal monochromatic collimated light source catered toward fetal visual perceptual parameters illuminate the uterine environment? (c) How might this stimuli present to the fetus? (d) How are these quantities affected by variation in adipose tissue? (e) To what extent does the horizontal separation distance along the maternal abdomen of multiple transdermal monochromatic collimated source stimuli affect how readily discernible the images are for the fetus?

Methodology

We use MC computational modeling to simulate the propagation of light from directed transdermal monochromatic collimated source stimuli through the abdominal tissue of a pregnant woman. No human tissues or samples were involved in this study. Consideration was given to use of the diffusion approximation in modeling; however, its validity is typically limited to situations where the light has been highly scattered[18] or the probability of scattering events is much greater than that of absorption events[19]. With the inclusion of amniotic fluid in our models, the diffusion approximation becomes relatively inaccurate when compared to methods such as MC modeling. Similarly, existing applications such as NIRFAST[20,21], which are dependent on diffusion approximations, may become less effective for our intended uses in modeling maternal tissue environments. This

can be further reasoned due to our close source proximity to the region of interest and the use of wavelengths outside the near-infrared wavelength range.

All simulations are ideally completed with model parameters relevant to the third trimester of pregnancy, as this is the optimum period for studying the development of the fetal eye via directed light stimuli. Hence, we have attempted to ensure optical parameters and layer thicknesses are derived from empirical data based on pregnant women at this stage of gestation. For certain aspects, however, the literature is not yet detailed enough to enable a definitive restriction of model parameters to any specific temporal stage of pregnancy. Consequently, though we attempt to limit used parameters to those found from third trimester pregnancies, some values are taken from the general population where appropriate data is unavailable. In cases where general population data is unavailable, values have been approximated from those available in the literature.

To run the simulations, we developed a computational model written in C17 standard C that follows a similar algorithm to that employed by the prominent Monte Carlo for Multi-Layered media (MCML)[22] model to run direct particle MC simulations. The primary reason for developing our own model was to incorporate aspects for computational efficiency such as Message Passing Interface (MPI) and to allow for streamlined customization related to our research group's applications in future work.

Our environmental model for this work is split into five layers: four representing the maternal tissues and one representing the amniotic fluid. Future experimental investigations by our group will deliver laser diode lights direct to the mother's skin, and the wavelength to be employed is 650 nm. This wavelength has been used in prior experimental work[7,13] and is chosen due to both its large tissue penetration depth (relative to shorter wavelengths) and its visibility to the human eye, which typically detects light in the range of 380 to 750 nm[23]. To demonstrate the benefit in terms of penetration depth for 650 nm, we simulate several monochromatic collimated light sources at wavelengths across this range, for which we have identified and incorporated relevant layer-dependent optical properties. The following wavelengths will be considered: 400 nm, 450 nm, 500 nm, 550 nm, 600 nm, 650 nm, and 700 nm. Optical parameters for these wavelengths are listed in Tables 1–3.

Lastly, to replicate the differences in tissue structure across individuals, we adjust the thickness of adipose tissue used in the model — the simulations use adipose thicknesses of 1.0 cm, 1.5 cm, 2.0 cm, and 2.5 cm. All other parameters are held constant.

The Monte Carlo model

The model follows a similar algorithm to that of MCML[22]. An input file describing the layers, their parameters, the beam, and several further simulation variables is read and a voxellated tissue region is generated to match the tissue's physical description. This allows for simple manipulation of the tissue to account for its heterogeneous nature. Hence, this voxellated approach is chosen to allow for future adaptation of the model to account for heterogeneity across the tissue of individuals. This will also enable the delivery of a consistent light source at the individual level for future experimental studies.

Photons are launched as packets with random, medium-specific path lengths and their propagation through to a tissue interaction site is simulated. The source is set as a single collimated photon beam launched orthogonally into the tissue at its surface. As the stimuli used in our wider research group's physical experiments has an incident beam diameter of 1.6 mm, we initiate the simulated source with a beam diameter of 1.6 mm, with photons randomly distributed across this region at launch. This size is typical of laser diodes for these applications. We use the Henyey-Greenstein[35] phase function to model the distribution of deflection angles in scattering:

$$p(\theta) = \frac{1}{4\pi} \frac{1 - g^2}{(1 + g^2 - 2g\cos(\theta))^{\frac{3}{2}}}, \tag{1}$$

while the azimuthal angle is sampled from a uniform distribution across the interval 0 to 2π. If the step of a packet will cross a boundary between tissue sublayers, transmission is determined by comparing a random number to the internal reflectance as computed by the Fresnel equations[36]:

$$r_{\perp} = -\frac{\sin(\theta_i - \theta_t)}{\sin(\theta_i + \theta_t)} \tag{2}$$

$$t_{\perp} = +\frac{2\sin(\theta_t)\cos(\theta_i)}{\sin(\theta_i + \theta_t)} \tag{3}$$

$$r_{\parallel} = +\frac{\tan(\theta_i - \theta_t)}{\tan(\theta_i + \theta_t)} \tag{4}$$

$$t_{\parallel} = +\frac{2\sin(\theta_t)\cos(\theta_i)}{\sin(\theta_i + \theta_t)\cos(\theta_i - \theta_t)}. \tag{5}$$

This is a common method employed in MC models (for example, see MCML[22]). In short, the above equations can be manipulated to give the local reflectance[37]:

$$R_i(\theta_i) = \frac{1}{2}\left(\frac{\sin^2(\theta_i - \theta_t)}{\sin^2(\theta_i + \theta_t)} + \frac{\tan^2(\theta_i - \theta_t)}{\tan^2(\theta_i + \theta_t)}\right), \tag{6}$$

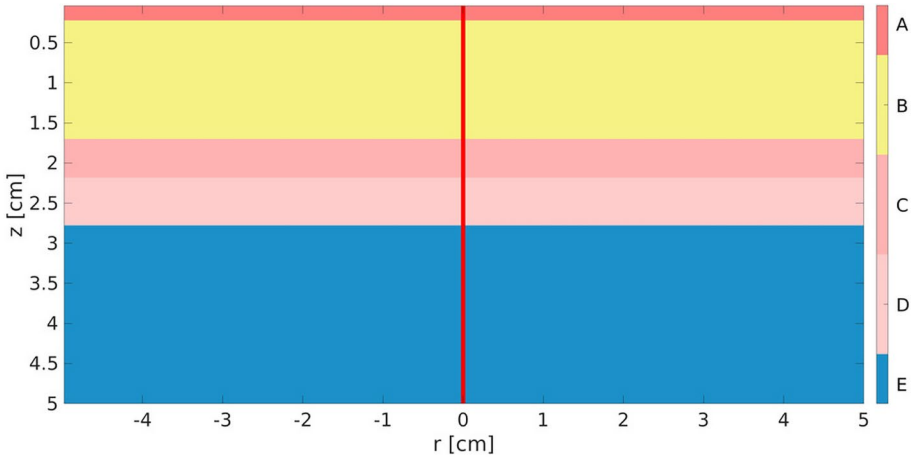

Fig. 1. Geometry of the layered tissue model used in our Monte Carlo simulations. Layer A is skin, Layer B is adipose, Layer C is muscle, Layer D is uterus, and Layer E is amniotic fluid.

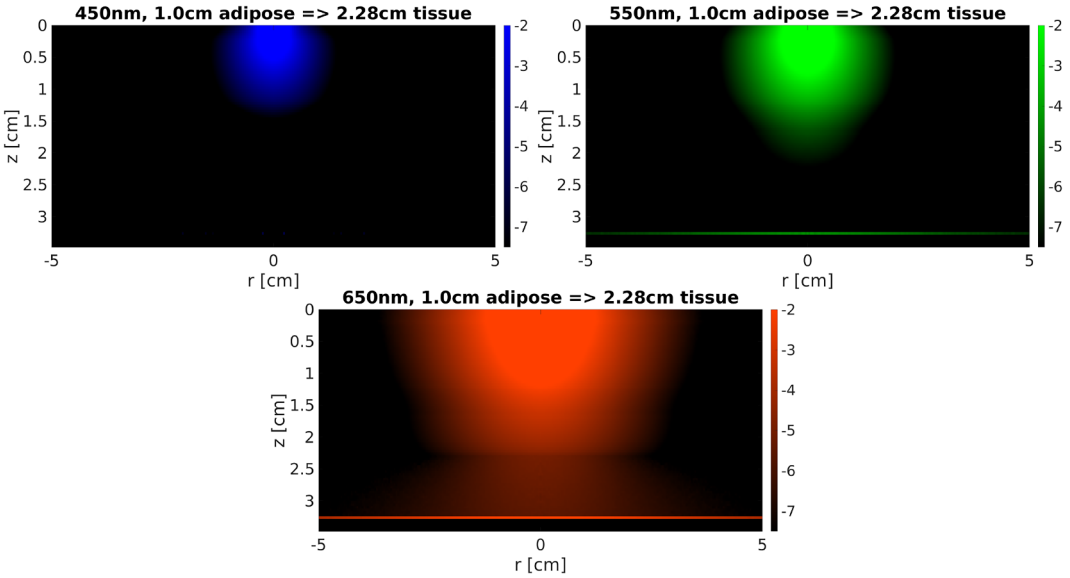

Fig. 2. Cross-sections of relative fluence rate (i.e., relative intensity, or watts of power incident per cm^2 per watt delivered) in the *r*-*z* plane for three select single beams of differing wavelength incident at the surface of the maternal abdominal skin. Note values are presented in base-10 logarithmic scale and the geometry is here presented in cylindrical coordinates.

where θ represents the angle of incidence or transmission depending on the subscript.

For the MC method, a pseudorandom number is generated and compared with $R_i(\theta_i)$ to decide whether the photon packet is reflected or transmitted. If the packet is internally reflected, its trajectory component perpendicular to the surface is reversed and it continues propagation in the current layer. If the packet is transmitted, its direction is updated according to the new layer's parameters and its propagation continues. This process repeats until the packet's weight reaches a predetermined lower bound and its termination is handled by a roulette process[38]:

$$W_1 = \begin{cases} kW_0 & \text{if} \quad \xi \leq \frac{1}{k} \\ 0 & \text{if} \quad \xi > \frac{1}{k}, \end{cases} \tag{7}$$

where k is typically chosen as 10[39], W_0 is the photon's current weight, W_1 is the updated weight, and ξ is a pseudorandom number in the interval $[0, 1]$.

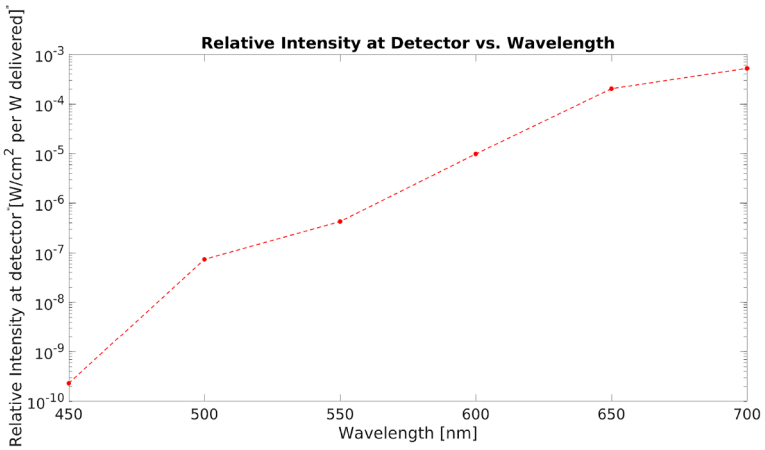

Fig. 3. Relative fluence rate (i.e., relative intensity, or watts of power incident per cm^2 per watt delivered) at the fetal detection layer for the seven wavelengths simulated.

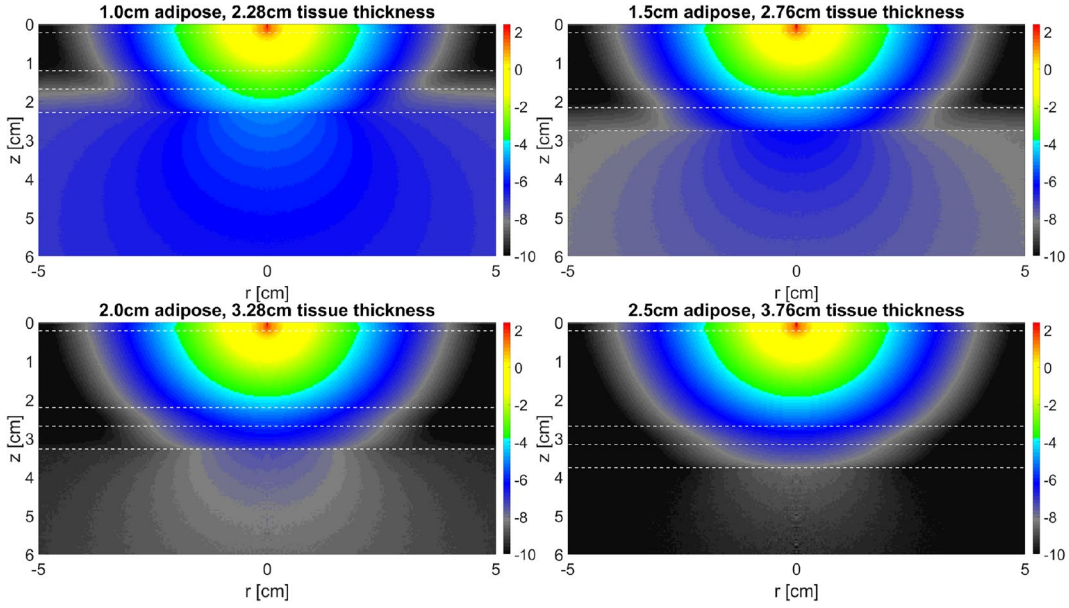

Fig. 4. Cross-sections of relative fluence rate (i.e., relative intensity, or watts of power incident per cm^2 per watt delivered) in the *r-z* plane for a single beam incident at the surface of the maternal abdominal skin, for varying adipose thicknesses. Dashed white lines represent layer boundaries outlined in Table 3. Values are presented in base-10 logarithmic scale and the geometry is in cylindrical coordinates.

The procedures are looped through until all packets have been simulated to their completion. At this stage, output data is written to a file which is read into Matlab scripts to generate images. For our later inspection of multiple beams, as the system used in these simulations is linear and invariant, we may simply shift the beam horizontally and sum the two response grids[40]. This component of the research is also handled by Matlab scripts before generating outputs.

To improve the model's computational efficiency, we incorporate parallel processing of photon trajectories. This is accomplished through use of the MPI standard, allowing faster processing of the 12 billion packages simulated per run. Data generated was benchmarked during model development against that produced by established models (such as MCML[22]) and found to be in good agreement. All simulations were conducted with 0.04 cm voxels.

Tissue model

We employ a four-layer tissue model for our simulations, consisting of skin, adipose, muscle, and uterus. Below the uterus layer is amniotic fluid. A *z*-plane cross-section of the tissue model used in our simulations is shown in Figure 1. Optical parameters for each layer are sourced for wavelengths at 50 nm increments across the visible spectrum. These are shown in Tables 1–3.

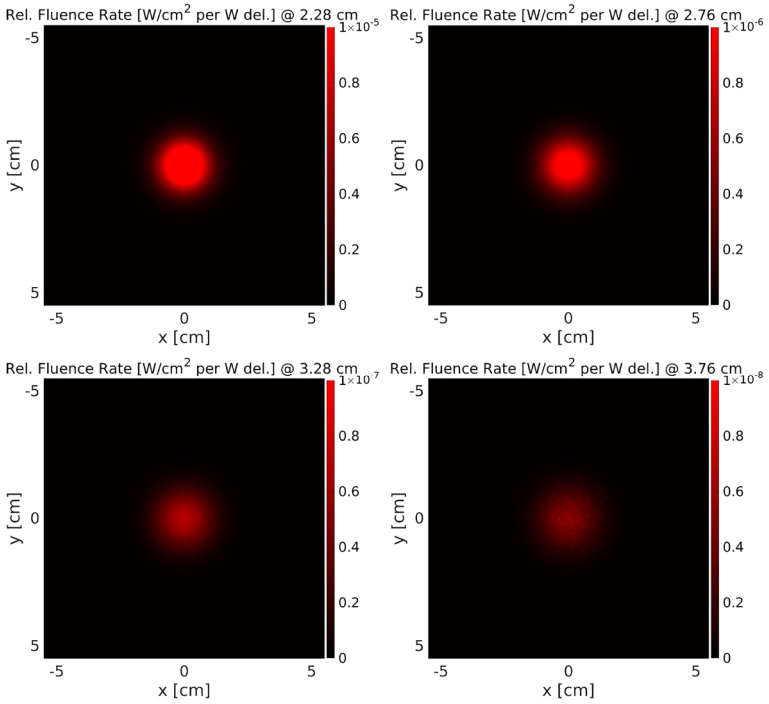

Fig. 5. Relative fluence rates [W/cm^2 per W delivered] for a single delivered beam. Images show relative intensity at the interface between tissue and amniotic fluid for varying thicknesses of adipose. Note the change in scale between figures.

The experimental side of this research requires the stage of fetal visual development to be sufficiently advanced enough to detect stimuli. Therefore, presentation of the laser diodes occurs during the third trimester of pregnancy and this needs to be accounted for in the tissue layer geometry. We have taken layer thickness values from empirical studies and these are shown in Table 3.

Results

Initial MC simulations model a single monochromatic beam's propagation through the tissue model. As we intend to use 650 nm stimuli in future experimental applications due to their visibility for the human eye and increased penetration depth in comparison to lower wavelength stimuli, we first simulate individual monochromatic collimated light sources at uniformly distributed wavelengths across the visible spectrum to demonstrate the improved penetration depth for 650 nm stimuli in maternal tissue.

Figure 2 shows cross-sections in the *r-z* plane of the relative fluence rate (i.e., relative intensity, or watts of power incident per cm^2 per watt delivered[41]) on a base-10 logarithmic scale for three select single beams in the range of 400 nm to 700 nm. For emphasis in these outputs, we have included a pseudo-fetal layer 1.0 cm below the tissue-fluid interface. In practice, the pseudo-fetal layer is not actually part of the tissue model — rather, it essentially acts as a detector layer to capture the residual energy carried by any photon packets which reach the simulated fetal depth, and this serves to provide an estimate on the energy reaching the fetus from light sources. Note all wavelengths are incident perpendicular to the surface of the maternal abdominal skin, the geometry is presented in cylindrical coordinates for these figures, and axial symmetry is assumed.

From inspection of Figure 2, it is evident that the wavelengths with greatest influence on light penetrating the uterus are those with higher magnitudes. From the intensities recorded at the fetal detection layers, for example, the 650 nm wavelength has the broadest presence while the 450 nm wavelength is minimally represented. Further, the intensity recorded by the fetal detector layer for each of the seven wavelengths simulated is shown in Figure 3. Note that the 400 nm wavelength did not reach the fetal detector layer, so it is not shown here. Again, there is a clear increase in intensity measured at the fetal detection layer as wavelength increases.

With justification for the use of 650 nm stimuli established, Figure 4 next shows cross-sections in the *r-z* plane of the relative fluence rate (i.e., relative intensity, or watts of power incident per cm^2 per watt delivered) on a base-10 logarithmic scale for a single 650 nm beam incident at the surface of the maternal abdominal skin, with each image displaying a different adipose thickness. The relationship evident from these images is that increased levels of adipose tissue thickness correspond to reduced levels of light intensity reaching the amniotic fluid. Note that the geometry is presented in cylindrical coordinates for these figures and axial symmetry is assumed.

Since a key objective of our work is to determine the appearance of transdermal monochromatic collimated source stimuli delivered to the fetus in utero, we present in Figure 5 the cross-sections of the simulated single beams' relative fluence rates in the *x-y* plane for varying adipose thicknesses (note the change to Cartesian coordinates for subsequent images, with no transformation conducted as the model tracks data on both cylindrical and Cartesian grids). Due to the variety of fetal eye positions in utero, it is unclear what position

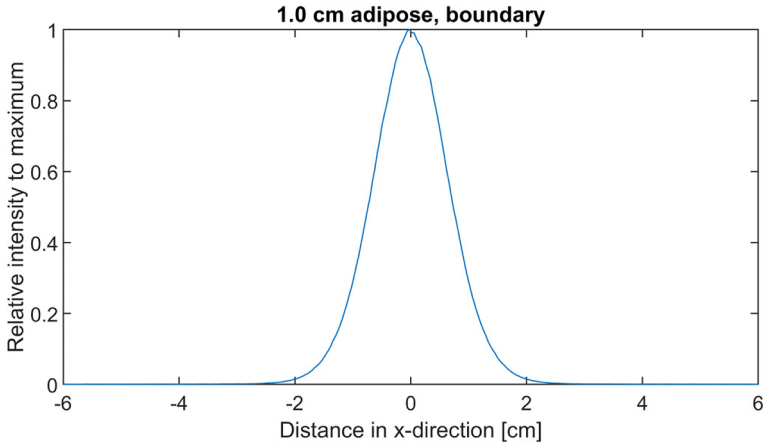

Fig. 6. Relative intensity of the single beam to its maximum intensity along the x-direction at $y = 0$ for the tissue profile with 1.0 cm adipose thickness at the interface between tissue and amniotic fluid. This gives an indication of the horizontal diffusion for a given transdermal monochromatic collimated stimuli after propagating through maternal tissue. Only the profile with 1.0 cm adipose thickness is shown. Similar plots generated for tissue profiles with thicker adipose result in noisier images (due to increased absorption impacting statistics) that reflect similar underlying distributions.

(relative to the tissue-amniotic fluid interface) is the ideal point to consider the simulated light intensity. We present a single option for consideration here: each image shows the beam's simulated relative fluence rate at the tissue-fluid interface for tissues with differing adipose thicknesses (in line with the source stimuli). This decision is due to the low absorption coefficient[11] and relatively low scattering coefficient[12] in amniotic fluid for the considered wavelength. Hence, we propose that light which reaches this interface is likely to continue propagating to the fetus with minimal attenuation — especially when noting that the typical separation between the fetal eye and the uterus is on the order of 1-2 cm[13].

As expected, the maximum relative intensity declines as adipose tissue thickness is increased. Adipose tissue typically has relatively high levels of absorption and scattering (see Tables 1 and 2) in comparison to other component layers represented in the model, such as skin and amniotic fluid, which leads to the large decline in relative intensity seen with increased adipose thickness. In contrast, amniotic fluid exhibits relatively low levels of absorption and scattering, leading to more noticeable diffusion of the photons that enter the uterine environment. The beam intensity is typically lower in the amniotic fluid than at the interface, with a broader geometric spread being evident. This is indicated by the widening of the intensity patterns shown in the amniotic fluid layers of Figure 4 (in particular, for the lesser adipose tissue thicknesses where more light is reaching the fluid), in contrast to the relatively narrow spreads within the tissue.

Figure 6 shows the intensity of the beam at the interface between tissue and amniotic fluid, relative to its maximum simulated intensity in the x-direction for $y = 0$ (i.e., the intensity simulated directly below the source delivery at this depth is normalized to 1.0). This plot gives an indication of the horizontal diffusion for a given transdermal monochromatic collimated stimuli after propagating through maternal tissue. Such information is useful for experimental applications where determining appropriate horizontal separation differences for transdermal stimuli on the maternal abdomen is required to ensure delivered stimuli remain visually distinct in the uterus. Note that larger adipose thicknesses result in visually similar beam profiles to that shown in Figure 6, so we simply present the first adipose thickness for consideration.

Figure 7 shows the decline in relative fluence rate along the z-axis for the four simulated adipose layer thicknesses. Due to the source location, the maximum values for intensity occur at the surface of the tissue ($z = 0$ cm). The fluence rates decrease with increasing z, as the beam propagates through more of the simulated tissue. Similar to previous studies[12], our model shows exponential trends (linear when on a logarithmic scale) for the decline in fluence rate over the tissue and amniotic fluid. As adipose tissue thickness increases, the decline in relative fluence rate by the tissue-fluid boundary becomes increasingly apparent. By taking the log values recorded at the tissue-fluid interface for each adipose thickness, inverting the log, and comparing the values for each thickness, we find that a reduction by 0.5 cm of adipose tissue results in, on average, an approximately 15 times larger eventual relative fluence rate measured at the tissue-fluid interface than before. For example, reducing adipose thickness from 2.5 cm to 2.0 cm results in a simulated relative fluence rate at the tissue-fluid interface approximately 15.5 times larger than that simulated with 2.5 cm of adipose tissue. Similar numbers are seen when reducing from 2.0 cm to 1.5 cm of adipose tissue and from 1.5 cm to 1.0 cm of adipose tissue.

In situ experimental designs motivating this modeling work will later involve moving two separate transdermal monochromatic light stimuli towards one another, without merging from the perspective of the fetus. We are interested, then, in knowing at what point two such stimuli cease to become notably distinct from each other. Consequently, we also model the appearance of two transdermal monochromatic stimuli presented to the fetus in utero, and the cross-sections of simulated x-y plane data for these are shown in Figures 8 and 9. Each row of images shows the relative fluence rates of two stimuli, as measured at the tissue-fluid interface.

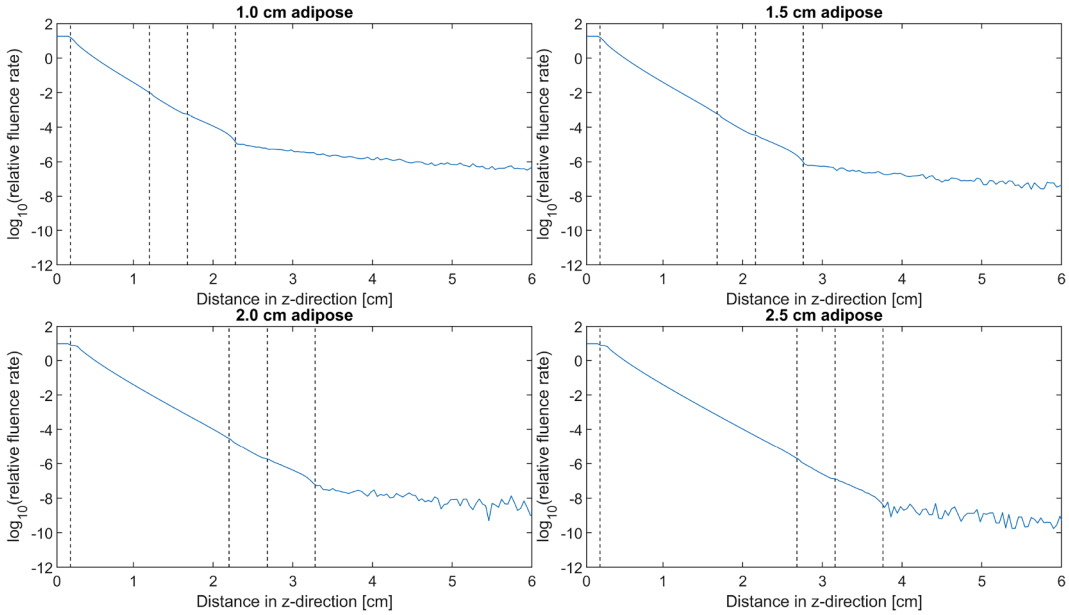

Fig. 7. Relative fluence rate vs. z-depth for different adipose tissue thicknesses. Note the relative fluence rates are presented in logarithmic scale. Vertical dashed lines represent boundaries between tissue layers, as defined in Table 3.

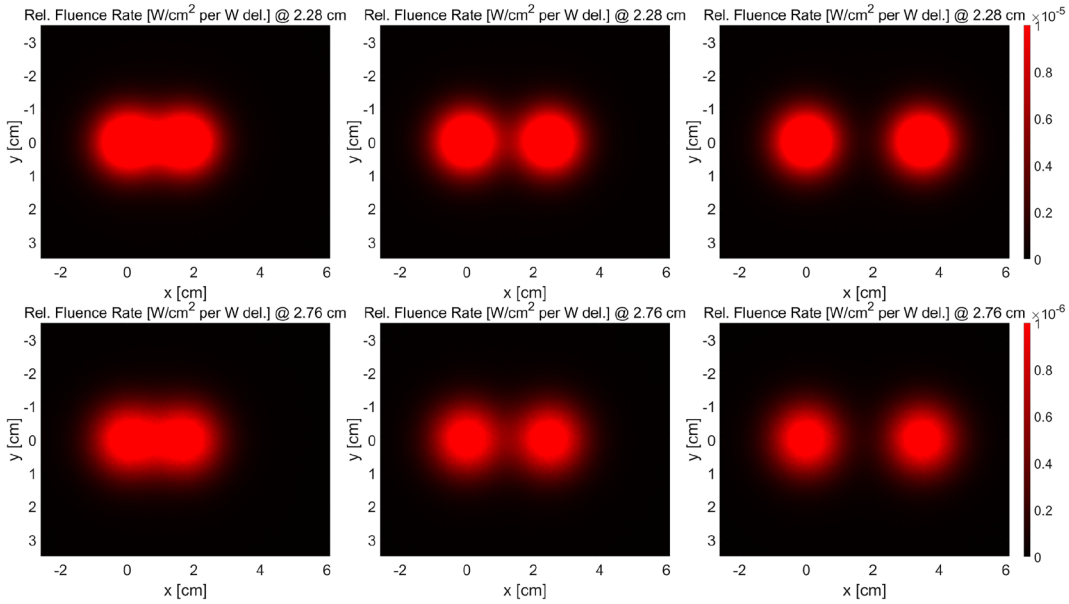

Fig. 8. Relative fluence rates [W/cm^2 per W delivered] for two stimuli. Left images show 18 mm stimuli separation, centre images 25 mm, and right images 35 mm. The top row is the relative fluence rate at the interface between tissue and amniotic fluid for 1.0 cm adipose, and the bottom row 1.5 cm adipose. Note the change in scale between figures.

We present three separation distances of the light sources for comparison: 18 mm, 25 mm, and 35 mm. These are based on proposed measurements employed for in situ psychological experiments[42]. In terms of intensity profiles, it is apparent that an 18 mm separation distance does not lead to noticeably distinct stimuli presentation for any tissue thickness simulated; however, there is reasonable distinction evident for simulations using the 25 mm separation distance, and the 35 mm separation distance appears to lead to noticeable intensity distinction for all simulated tissue thicknesses.

Similar to Figure 6, the graphs presented in Figure 10 show the profiles of simulated intensity relative to maximum intensity for two beams. As in Figures 8 and 9, these are measured along the centre of the x-y plane

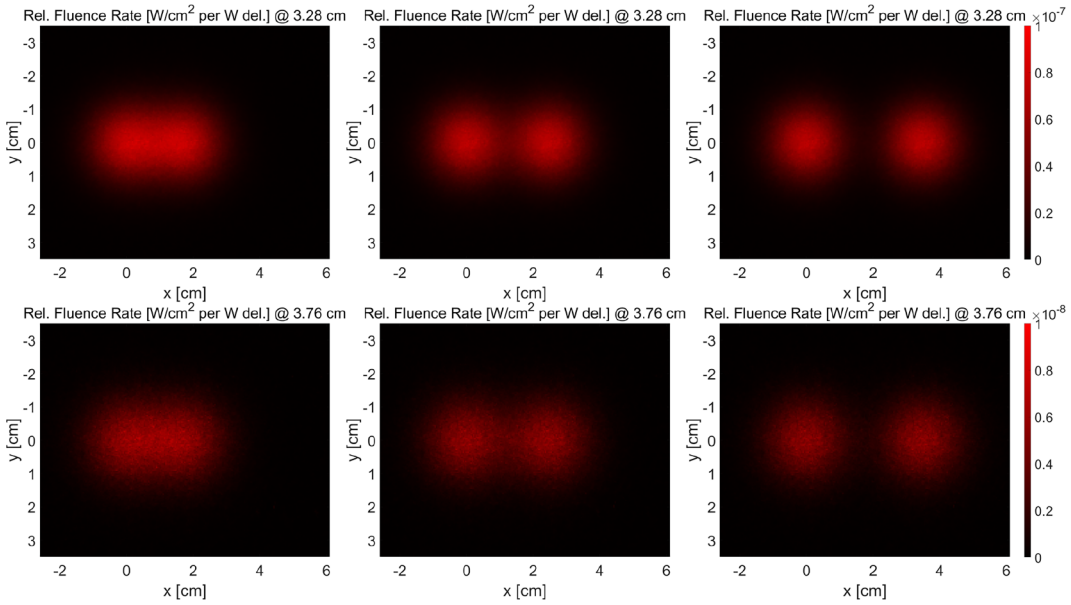

Fig. 9. Relative fluence rates [W/cm^2 per W delivered] for two stimuli. Left images show 18 mm stimuli separation, centre images 25 mm, and right images 35 mm. The top row is the relative fluence rate at the interface between tissue and amniotic fluid for 2.0 cm adipose, and the bottom row 2.5 cm adipose. Note the change in scale between figures.

at the tissue-fluid interface. Again, simulated separation distances of 18 mm, 25 mm, and 35 mm are applied at the sources.

As expected, moving the sources closer together causes the intensity distinction between the two beams to be reduced. As adipose tissue thickness is increased, the distinction between the beams at the tissue-fluid interface is steadily reduced, with the 18 mm source separation only showing minimal distinction in the peaks for the 1.0 cm adipose tissue (shown in Figure 10), while the 25 mm separation appears to maintain distinct intensity plots when measured at the interface until the adipose tissue is increased to 2.5 cm. The 35 mm separation consistently produces distinguishable images at the tissue-fluid interface across all thicknesses, demonstrated in Figures 9 and 10, with the relative intensity to maximum dropping below 0.2 between the simulated stimuli at the tissue-fluid interface. Note again that larger adipose thicknesses result in qualitatively similar beam profiles to that shown in Figure 10, so we simply present the first adipose thickness for consideration.

Discussion

We first use MC simulations to demonstrate the relationship between increasing wavelength (across the visible spectrum of light) and the propagation of monochromatic collimated light source laser diode stimuli presented to the maternal abdomen and, consequently, the fetus in utero. As the wavelength of light simulated increases across the visible spectrum, light intensity levels reaching the fetus typically increase. For example, comparing the results for the 450 nm wavelength to those of the 650 nm wavelength in Figure 2 shows a clear increase in light intensity at increasingly greater penetration depths of the maternal tissue and amniotic fluid. This is further shown in Figure 3. Typically, for biological tissue, one would expect penetration depth to increase with wavelength across the visible spectrum[43], and these results are in line with this expectation.

We then demonstrate the relationship between increasing thicknesses of adipose tissue and the attenuation of transdermal monochromatic collimated source laser diode stimuli presented to the human fetus in utero. In general, the levels of light intensity reaching the fetus decrease with increasing adipose thickness. For example, comparing the results for the 1.0 cm adipose thickness to those of the 2.5 cm adipose thickness in Figure 7 shows the former experiences relative fluence rates at the tissue-fluid interface approximately 3, 500 times larger than the latter. This is further demonstrated by the apparent decline in intensity exhibited by the beam profiles at the tissue-fluid interface in Figure 5— the scale from the 1.0 cm adipose thickness to the 2.5 cm adipose thickness falls dramatically, and this is representative of the significant attenuation of simulated photon packets due to increased adipose influence on propagation.

It is important to note that most of the images provided thus far display measurements of relative light intensity. In other words, the incident power (in watts) per unit area (in cm^2) per unit power presented (in watts). For example, the log value shown in Figure 7 at the tissue-fluid interface along the z-axis is approximately -7.22 for the 2.0 cm adipose thickness, indicating a simulated relative fluence rate of 6.03×10^{-8} W/cm^2 per W delivered. Using the 5 mW power presented to the tissue, we find a simulated fluence rate of 3.01×10^{-10} W/cm^2 for this incident power. As noted, this is a measure of intensity; however, it does not give an intuitive indication of how "bright" this stimuli may appear to the fetus. In order to interpret the stimuli from this alternative perspective, we need to convert the simulated intensity to illuminance. This can be handled in a relatively simple

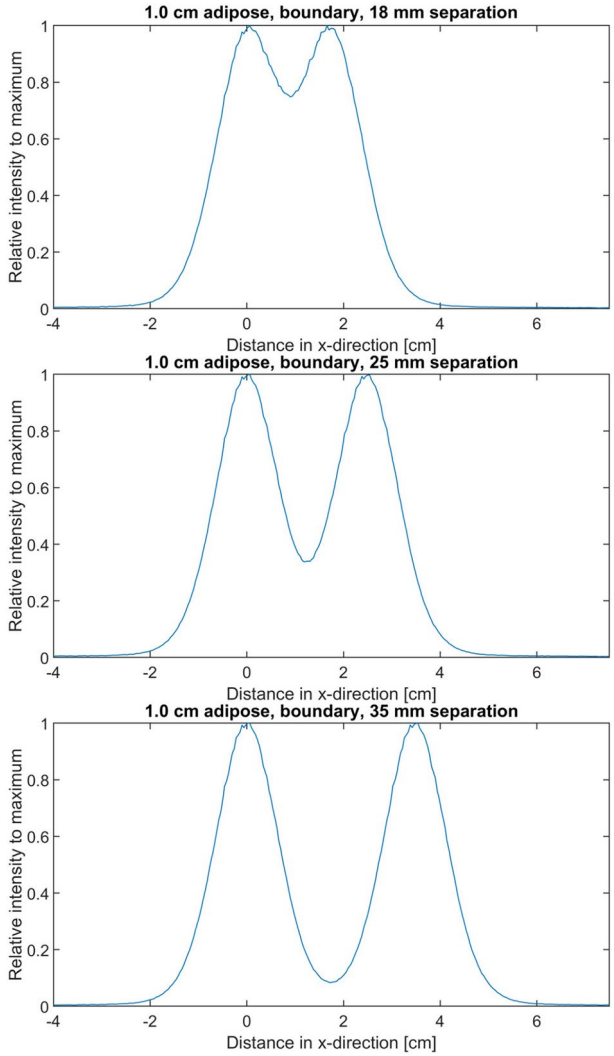

Fig. 10. Relative intensity of the two beams to their maximum intensity along the x-direction at $y = 0$ for the tissue profile with 1.0 cm adipose thickness at the interface between tissue and amniotic fluid. The top image shows an 18 mm stimuli separation, the centre image a 25 mm separation, and the bottom image a 35 mm separation. Only the profile with 1.0 cm adipose thickness is shown. Similar plots generated for tissue profiles with thicker adipose result in noisier images (due to increased absorption impacting statistics) that reflect similar underlying distributions.

manner to ascertain an approximate value that can be interpreted by way of comparison to more common sources of illuminance.

The conversion of intensity (irradiance) in units of Watts/m^2 to illuminance in units of lux can be performed using the following formula[44]:

$$\text{lux} = 683.002 \cdot \int_0^\infty E(\lambda)\, \bar{y}(\lambda)\, \mathrm{d}\lambda, \tag{8}$$

where 683.002 is the constant representing the maximum spectral luminous efficacy and is measured in lm/W; $E(\lambda)$ is the intensity (irradiance) spectrum measured in W/m^2 per nm, which is taken from the simulation results; $\bar{y}(\lambda)$ represents either the photopic (light-adapted) or scotopic (dark-adapted) luminosity function of wavelength for humans; and the integral is taken over the spectrum of simulated wavelengths. For our single wavelength simulations, we integrate over a Dirac delta function. Hence, the conversion equation becomes simply

$$\text{lux} = 683.002 \cdot E(\lambda)\, \bar{y}(\lambda)\,. \tag{9}$$

The distinction between using the photopic or scotopic luminosity function involves the levels of light under consideration — for everyday light levels, the response of the human eye is most appropriately approximated

Adipose thickness [cm]	Tissue thickness [cm]	Log at interface	Photopic [lx]	Scotopic [lx]	Photopic comparison
1.00	2.28	-4.85	5.16×10^{-2}	3.27×10^{-4}	Quarter moon–Full moon, clear conditions
1.50	2.76	-6.03	3.41×10^{-3}	2.16×10^{-5}	Clear, starry sky–Quarter moon
2.00	3.28	-7.22	2.20×10^{-4}	1.39×10^{-6}	Overcast night sky–Clear, starry sky
2.50	3.76	-8.41	1.42×10^{-5}	8.99×10^{-8}	Overcast night sky

Table 4. Illuminances determined by simulations at the tissue-fluid interface for various adipose tissue thicknesses.

by the photopic luminosity function, while the scotopic luminosity function is most applicable in low light conditions. Consequently, one might initially expect the uterine environment to correspond to one where the scotopic function is most relevant; however, it is unclear exactly what levels of light might already be present in the uterus due to natural light sources. Similarly, the development of the fetal eye (and its adaptation to the uterine environment) is presently not well known. Assuming low light levels would likely offer the safest and most reasonable starting estimate, and this indicates use of the scotopic function may be appropriate for our purposes.

Taking, for example, our previously mentioned value of 3.01×10^{-10} W/cm^2 at the tissue-fluid interface for 2.0 cm adipose thickness, converting this to W/m^2 to find E(650 nm), and substituting this value into the equation with $\bar{y}$(650 nm) = 0.107 for the photopic function at 650 nm or 0.000677 for the scotopic function at 650 nm[45], we calculate illuminances of 2.2×10^{-4} lx or 1.4×10^{-6} lx, respectively. The former is roughly between the illuminance levels of an overcast night sky and a clear, starry night sky[46], while the latter is not immediately comparable to any common illuminance level. This suggests that illuminance levels provided to the uterine wall by the simulated stimuli are unlikely to offer a noticeable illuminance for the fetus when adipose tissue thickness is 2.0 cm or above.

In contrast, however, taking the simulated tissue-fluid interface relative fluence rate from Figure 7 for the 1.0 cm adipose thickness and applying the same calculation gives a result of approximately 0.05 lx for the photopic function, which is an illuminance approximately between a full moon in clear conditions or a quarter moon[46]. Using the scotopic function as above results in a calculated illuminance of 3.27×10^{-4} lx, which is between the levels of illuminance exhibited by an overcast night sky and a clear, starry night sky[46]. These values, and those as calculated for the simulations involving all other tissue thicknesses, are summarized in Table 4 alongside their counterpart values taken from simulating light propagation into the amniotic fluid. In general, the conclusion drawn from these simulations is that the uterine wall is reasonably illuminated under these conditions for adipose tissue thicknesses of 1.0 cm to 1.5 cm, but adipose thicknesses of 2.0 cm and above seem unlikely to offer noticeable uterine wall illumination. Similarly, due to the nature of amniotic fluid, levels of illuminance from the given transdermal stimuli with 1.0 cm or 1.5 cm adipose tissue thickness would seem likely to remain reasonably high upon reaching the fetus.

To further validate usage of the 650 nm wavelength in stimuli presented to the fetus via the maternal abdominal exterior, we next compare the consequent illuminances determined from values in Figure 3. We find that the illuminances calculated at the fetal detection layer for 1.0 cm adipose thickness range from 5.84×10^{-10} lx for the 450 nm stimulus to 1.35×10^{-3} lx for the 700 nm stimulus. Note that no light was detected at the detection layer for the 400 nm stimulus, and that these values are calculated with the scotopic function, which provides a lower, potentially more realistic estimate than the photopic function. The former value is not readily comparable to any common illuminance level, while the latter is between that of a clear, starry sky and a quarter moon[46]. The remaining simulated wavelengths between 450 nm and 700 nm show increasing illuminance as wavelength increases; however, the lowest to be comparable to a common illuminance level is 600 nm at 2.82×10^{-5} lx, which is comparable to an overcast night sky[46]. These values further support the choice of 650 nm for the experimental stimulus based on light reaching the fetus. In addition, these results suggest a stimulus between 600 nm and 700 nm provides sufficient intensity to the fetus (in the 1.0 cm adipose case) to be potentially visible. This would, of course, depend on the precise capabilities of the fetal eye, though values may be higher if the photopic function is more applicable. Further, 700 nm is relatively close to the edge of the visible spectrum, so stimuli at this wavelength may not provide the intended visible image to the fetus.

Note that the prior discussion does not counter the limited scope for fetal ability to individuate transdermal stimuli with smaller separation distances. Though the illuminance offered by a single laser diode collimated light source may be evident to the fetus, the likelihood of the fetus being able to discern separate equivalent transdermal monochromatic light sources when presented in close proximity to one another — less than 25mm, for instance — is heavily impacted by attenuation in the maternal tissue (particularly from adipose tissue). Similarly, additional diffusion in the amniotic fluid further complicates this aspect. Consequently, it is possible that fetuses developing in uterine environments with moderately thick adipose tissue layers are able to see such transdermal stimuli presented, yet they are unable to recognize the stimuli as distinct sources of light if their delivery separation distance is not sufficiently large on the maternal abdomen.

Despite the reasonable likelihood of certain transdermal monochromatic laser diode stimuli reaching the fetus and illuminating the womb, the argument of whether the fetal eye and brain are developed enough to recognize or respond to the stimuli is one which needs to be considered when applying these results. In general, experimental work in the field of fetal vision focuses on third trimester fetuses. It has been shown that the fetal

eye develops late in pregnancy[13], and the fetus is capable of responding to transdermal laser diode stimuli after 34 weeks of pregnancy[14]. Hence, although it is not the focus of this paper, any interpretation of these results from the perspective of fetal recognition should consider only the third trimester of gestation — the applicability to fetal recognition in earlier stages of development is not yet well known.

In addition, the typical separation between the fetal eye and the uterus is on the order of 1-2 cm[13], and this is unlikely to align with the near point of the fetus (though there is presently no information in this area). The work we have performed does not claim that the fetus is able to focus on the uterine wall — rather, it is likely that stimuli would be out of focus for the fetus given the typical separation distance. Despite this, developmental methods for measuring visual acuity such as the optokinetic nystagmus[47] and preferential looking[48], have never been employed with a fetal sample. It should also be recognised that ideal acuity is not required for the individuation of two stimuli prior to the fetal near point, as we have attempted to simulate earlier in this paper. This is also the case for other aspects of visual information processing where nonfoveated space is normative, such as the visual periphery[49].

An important conclusion that can be drawn from these simulations pertains directly to the experimental component of this wider research and the field of fetal visual development in general. Our group is interested in the visual capabilities of the human fetus, and this is most readily examinable through delivering laser diode stimuli to the uterus and recording fetal response via ultrasound or heart rate. Based on the results of our model, experiments of this nature clearly face constraints in the delivery of stimuli to the fetus, including low levels of illuminance delivered for some adipose tissue thicknesses and the poor uterine distinction of multiple stimuli presented to individuals with higher adipose thickness. Consequently, this knowledge can serve to inform future experimental design in at least four ways.

First, stimuli within the 600 nm to 700 nm range are most likely to penetrate the maternal tissue sufficiently to provide illuminance to the fetus that is comparable to more common lighting scenarios. Preference toward 650 nm stimuli is reasonable, given both the relatively low illuminance calculated from the simulated 600 nm source and the proximity of 700 nm to the visible spectrum's end suggesting the fetal eye may struggle to detect the image.

Second, the 5 mW incident power used in these experiments appears to be on the low end of what is capable of delivering stimuli to the average fetus. A stronger laser diode (within the range of safe power levels) would result in brighter stimuli presentation to the fetus; however, this evidently poses potential danger to both the fetal eye and the mother's skin due to heat output from the light source.

Third, the poor propagation of simulated light through thicker adipose layers suggests an effective screening mechanism when identifying candidates for experimental participation. Such an approach could involve measuring abdominal tissue composition via ultrasound to exclude those with high adipose thicknesses. Alternatively, the measuring of a "no response" outcome during stimuli experiments might suggest that the mother was an inappropriate candidate for the utilized light source. This may be further verified by examining data taken from the ultrasound readings and categorising "no response" participants based on tissue composition.

Fourth, experimental applications involving multiple transdermal monochromatic light sources need to carefully consider placement along the maternal abdomen — stimuli with separation distances less than 25 mm evidently will face a large degree of "blurring" across the delivered stimuli, dependent on the exact fetal eye location (and its covering), and this can pose significant problems for experimental design and the conclusions drawn.

Future work should consider the influence of varying the muscle and uterus layers simulated. These layers also exhibit high absorbing and scattering properties, respectively, and though their significance in the overall tissue composition is not as prominent as that of adipose, their thicknesses do vary across individuals. Similarly, the thickness of these layers has a temporal aspect (like adipose tissue), with the stage of gestation also noticeably affecting their prominence. As an example, the maternal muscle structure stretches and separates during the late stages of pregnancy due to the growth of the fetus[50]. Hence, models that include a layer of muscle at the abdominal apex may overestimate the attenuation of light from this direction, and future modeling should consider this temporal aspect. There is also an argument to be made for accounting for skin color in the model, as melanin is highly absorbing in this part of the light spectrum. Consideration of these aspects with alterations made in a similar manner to those shown in this work would further illuminate their significance in determining the levels of light reaching the fetus.

Further, this work has assumed the fetal eye is open when determining transdermal stimuli appearances in utero (i.e., attenuation has not been simulated through an eyelid). Of course, the presence of an additional layer of skin would introduce further attenuation of the light source simulated. Due to the nature of the fetal sleep cycle and practical constraints, it is difficult to align experimental participants with times where the fetal eye is definitely open and exposed. Hence, the exact applicability of this present study to experimental situations where the fetal eye is closed needs to be considered carefully. Future work should introduce an additional layer to represent the eyelid in order to offer information on these situations. The presence of clothing (and similar additional layers) could also be considered in future simulations akin to this work; however, in situ studies exploring the development of fetal vision typically require direct skin contact for stimuli delivery, so similar applicability to the wider research field would be limited in comparison to that of this work.

Lastly, we have here simulated collimated sources in instances where the abdominal tissue is assumed to be locally flat (planar). In reality, the maternal abdomen exhibits curvature and this change in geometry would presumably have some impact on the results for situations where stimuli were not presented in such close proximity to one another. Future modeling work intends to account for this aspect alongside the points noted above.

Conclusion

The modeling presented in this paper offers quantitative data via MC simulations which further indicate that the human uterine environment can be at least partially illuminated via appropriate laser diode stimuli presented to the maternal abdomen. We have developed our own model of photon propagation through maternal abdominal tissue in line with common algorithms within the field and incorporated computational approaches that allow for efficient simulation of large numbers of photon packets (beyond 12 billion per run).

Results from the performed simulations suggest stimuli delivered to the fetus via the maternal abdominal exterior should be within the range of 600 nm to 700 nm to improve the likelihood of fetal detection, with 650 nm potentially providing the ideal stimuli when considering the development of the fetal eye, the relatively low illuminance provided by 600 nm stimuli, and the proximity of 700 nm to the edge of the visible spectrum. The intensity of light and consequent illuminance delivered to the fetus is found to vary strongly with maternal abdominal adipose thickness, and our simulations show that collimated transdermal monochromatic stimuli delivery to the fetus can result in illuminance comparable to that of a full moon for lower adipose thicknesses and a 650 nm source.

Increased adipose thickness causes light to be heavily attenuated, and this strongly degrades the delivered stimuli; however, the simulations suggest consideration of stronger incident stimuli (within the realms of fetal and maternal safety) would improve uterine illuminance. Further, the work of this paper suggests an appropriate screening tool for participants in fetal visual stimuli experiments could involve measuring abdominal adipose thickness of the mother; if stimuli are unable to be adjusted to improve photon penetration, the results of this modeling support excluding results from these participants due to low levels of delivered uterine illuminance.

Lastly, we have explored the potential to deliver multiple distinct transdermal monochromatic stimuli to the fetus in line with our research group's experimental design. The results of our simulations suggest that, from the three separation distances proposed for multiple stimuli: a distance of 18 mm is unlikely to produce distinct visual stimuli for the fetus, a distance of 35 mm is likely to generate visually distinct stimuli, and a distance of 25 mm may produce visually distinct stimuli for the fetus (though this depends on the precise capabilities of the fetal visual system which are presently unknown). Again, usage of a more powerful laser diode light source would ensure the presented images are visible for fetal eyes resting further into the amniotic fluid; however, any increase in power would need to be handled with caution and strong regard for safety requirements due to potential danger imposed to both the fetal eye and maternal skin.

This work has focused on varying adipose thickness; however, future studies will also investigate the required stimuli separation distances (and attenuation of stimuli) under varying muscle and uterus thicknesses. In addition, there is scope to explore the extension of collimated light sources to a range of alternate stimuli.

Data availability

All data from the simulations performed within is available upon reasonable request from the corresponding author.

Received: 1 February 2024; Accepted: 10 September 2024
Published online: 18 February 2025

References

1. Bradley, R. M. & Mistretta, C. M. Fetal sensory receptors. *Physiological Reviews* **55**, 352–382 (1975).
2. Lecanuet, J. & Schaal, B. Fetal sensory competencies. *European Journal of Obstetrics & Gynecology and Reproductive Biology* **68**, 1–23 (1996).
3. Myowa-Yamakoshi, M. & Takeshita, H. Do human fetuses anticipate self-oriented actions? a study by four-dimensional (4d) ultrasonography. *Infancy* **10**, 289–301 (2006).
4. Liley, A. W. The foetus as a personality. *Australian & New Zealand Journal of Psychiatry* **6**, 99–105 (1972).
5. Jacques, S., Weaver, D. & Reppert, S. Penetration of light into the uterus of pregnant mammals. *Photochemistry and Photobiology* **45**, 637–641 (1987).
6. Giudice, M. D. Alone in the dark? modeling the conditions for visual experience in human fetuses. *Developmental Psychobiology* **53**, 214–219 (2011).
7. Reid, V. M. et al. The human fetus preferentially engages with face-like visual stimuli. *Current Biology* **27**, 1825–1828 (2017).
8. Rao, S. et al. A direct and melanopsin-dependent fetal light response regulates mouse eye development. *Nature* **494**, 243–246 (2013).
9. Yang, M. B., Rao, S., Copenhagen, D. R. & Lang, R. A. Length of day during early gestation as a predictor of risk for severe retinopathy of prematurity. *Ophthalmology* **120**, 2706–2713 (2013).
10. Jacques, S., Ramanujam, N., Vishnoi, G., Choe, R. & Chance, B. Modeling photon transport in transabdominal fetal oximetry. *Journal of Biomedical Optics* **5**, 277–82 (2000).
11. Scheel, A. M., Ritchie, S. J., Brown, N. & Jacques, S. L. Methodological problems in a study of fetal visual perception. *Current Biology* **28**, R594–R596 (2018).
12. Gunther, J. et al. Effect of the presence of amniotic fluid for optical transabdominal fetal monitoring using Monte Carlo simulations. *Journal of Biophotonics* **14** (2021).
13. Donovan, T., Dunn, K., Penman, A., Young, R. J. & Reid, V. M. Fetal eye movements in response to a visual stimulus. *Brain and Behavior* **10**, e01676 (2020).
14. Dunn, K., Reissland, N. & Reid, V. M. The functional foetal brain: a systematic preview of methodological factors in reporting foetal visual and auditory capacity. *Developmental Cognitive Neuroscience* **13**, 43–52 (2015).
15. Kennedy, N. J. et al. Maternal abdominal subcutaneous fat thickness as a predictor for adverse pregnancy outcome: a longitudinal cohort study. *BJOG: An International Journal of Obstetrics & Gynaecology* **123**, 225–232 (2016).
16. D'Ambrosi, F. et al. Maternal subcutaneous and visceral adipose ultrasound thickness in women with gestational diabetes mellitus at 24–28 weeks' gestation. *Fetal Diagnosis and Therapy* **43**, 143–147 (2017).
17. Hwang, M. S. Abdominal skin subcutaneous fat thickness over the gestational period in korean pregnant women: a descriptive observational study. *Korean Journal of Women Health Nursing* **27**, 318–325 (2021).
18. Welch, A. J. & van Gemert, M. J. C. *Optical-thermal response of laser-irradiated tissue* (Springer, Netherlands, 2011).

19. Duderstadt, J. J. & Hamilton, L. J. *Nuclear Reactor Analysis* (Wiley, 1976).
20. Dehghani, H. et al. Near infrared optical tomography using nirfast: algorithm for numerical model and image reconstruction. *Communications in Numerical Methods in Engineering* **25**, 711–732 (2009).
21. Jermyn, M. et al. Fast segmentation and high-quality three-dimensional volume mesh creation from medical images for diffuse optical tomography. *Journal of Biomedical Optics* **18** (2013).
22. Wang, L., Jacques, S. L. & Zheng, L. MCML – Monte Carlo modeling of light transport in multi-layered tissues. *Computer Methods and Programs in Biomedicine* **47**, 131–146 (1995).
23. Starr, C. *Biology: Concepts and Applications* (Thomson, Brooks/Cole, 2005).
24. Torricelli, A., Pifferi, A., Taroni, P., Giambattistelli, E. & Cubeddu, R. In vivo optical characterization of human tissues from 610 to 1010 nm by time-resolved reflectance spectroscopy. *Physics in Medicine & Biology* **46**, 2227–37 (2001).
25. Bashkatov, A. N., Genina, E. A., Kochubey, V. I. & Tuchin, V. V. Optical properties of the subcutaneous adipose tissue in the spectral range 400–2500 nm. *Optics and Spectroscopy* **99**, 836–842 (2005).
26. Shimojo, Y., Nishimura, T., Hazama, H., Ozawa, T. & Awazu, K. Measurement of absorption and reduced scattering coefficients in Asian human epidermis, dermis, and subcutaneous fat tissues in the 400- to 1100-nm wavelength range for optical penetration depth and energy deposition analysis. *Journal of Biomedical Optics* **25** (2020).
27. Simpson, C. R., Kohl, M., Essenpreis, M. & Cope, M. Near-infrared optical properties of ex vivo human skin and subcutaneous tissues measured using the monte carlo inversion technique. *Physics in Medicine & Biology* **43**, 2465–78 (1998).
28. Marchesini, R., Bertoni, A., Andreola, S. A., Melloni, E. & Sichirollo, A. E. Extinction and absorption coefficients and scattering phase functions of human tissues in vitro. *Applied optics* **28**, 2318–24 (1989).
29. Ripley, P. M., Laufer, J. G., Gordon, A. D., Connell, R. J. & Bown, S. G. Near-infrared optical properties of ex vivo human uterus determined by the monte carlo inversion technique. *Physics in Medicine & Biology* **44**, 2451–62 (1999).
30. Buiteveld, H., Hakvoort, J. & Donze, M. Optical properties of pure water. *Proc. SPIE 2258, Ocean Optics* **XII** (1994).
31. Bashkatov, A. N., Genina, E. A. & Tuchin, V. V. Optical properties of skin, subcutaneous, and muscle tissues: a review. *Journal of Innovative Optical Health Sciences* **04**, 9–38 (2011).
32. Fukano, M. et al. Recovery of abdominal muscle thickness and contractile function in women after childbirth. *International Journal of Environmental Research and Public Health* **18**, 1–9 (2021).
33. Durnwald, C. P. & Mercer, B. M. Myometrial thickness according to uterine site, gestational age and prior cesarean delivery. *The Journal of Maternal-Fetal & Neonatal Medicine* **21**, 247–250 (2008).
34. Meglinski, I. V. & Matcher, S. J. Quantitative assessment of skin layers absorption and skin reflectance spectra simulation in the visible and near-infrared spectral regions. *Physiological Measurement* **23**, 741 (2002).
35. Henyey, L. G. & Greenstein, J. L. Diffuse radiation in the Galaxy. *The Astrophysical Journal* **93**, 70–83 (1941).
36. Smith, D. *Field Guide to Physical Optics*, 30–31. Field Guides (SPIE Press, 2013).
37. Hecht, E. *Optics, 4th Edition* (Pearson plc, 2001).
38. Dunn, W. L. & Shultis, J. K. 5 - variance reduction techniques. In Dunn, W. L. & Shultis, J. K. (eds.) *Exploring Monte Carlo Methods*, 97–132 (Elsevier, Amsterdam, 2012).
39. Jacques, S. L. Monte carlo modeling of light transport in tissue (steady state and time of flight). In Welch, A. J. & van Gemert, M. J. C. (eds.) *Optical-Thermal Response of Laser-Irradiated Tissue*, 109–144 (Springer Netherlands, 2011).
40. Wang, L., Jacques, S. L. & Zheng, L. Conv–convolution for responses to a finite diameter photon beam incident on multi-layered tissues. *Computer Methods and Programs in Biomedicine* **54**, 141–150 (1997).
41. Jacques, S. L. Modeling tissue optics using Monte Carlo modeling: a tutorial. In Jacques, S. L., Roach, W. P. & Thomas, R. J. (eds.) *Optical Interactions with Tissue and Cells XIX*, vol. 6854, 68540T. International Society for Optics and Photonics (SPIE, 2008).
42. Reid, V. M. & Dunn, K. The fetal origins of human psychological development. *Current Directions in Psychological Science* **30**, 144–150 (2021).
43. Finlayson, L. et al. Depth penetration of light into skin as a function of wavelength from 200 to 1000 nm. *Photochemistry and Photobiology* **98**, 974–981 (2022).
44. Johnsen, S. *The optics of life: a biologist's guide to light in nature* (Princeton University Press, 2012).
45. Williamson, S., Cummins, H. Z. & Kidder, J. N. *Light and color in nature and art* (John Wiley & Sons, 1983).
46. Rich, C. & Longcore, T. *Ecological consequences of artificial night lighting* (Island Press, 2006).
47. Dobson, V. Behavioral tests of visual acuity in infants. *International Ophthalmology Clinics* **20**, 233–250 (1980).
48. Teller, D. Y. Measurement of visual acuity in human and monkey infants: the interface between laboratory and clinic. *Behavioural Brain Research* **10**, 15–23 (1983).
49. Boucart, M. et al. Finding faces, animals, and vehicles in far peripheral vision. *Journal of Vision* **16**, 10–10 (2016).
50. Gilleard, W. L. & Brown, J. M. M. Structure and function of the abdominal muscles in primigravid subjects during pregnancy and the immediate postbirth period. *Physical Therapy* **76**, 750–762 (1996).

Acknowledgements

This work is funded by the Royal Society Marsden Fund (UOW2005).

Author contributions

ZI developed the model, conducted the literature research, performed the MC simulations and subsequent analysis, and drafted the paper. JH supervised the work, assisted with model development and analysis of the data, and also helped with drafting the paper. VR provided input into the developmental psychology and experimental background and assisted with drafting the paper.

Competing interests

The authors declare no competing interests.

Additional information

Correspondence and requests for materials should be addressed to Z.I.